This is an author's preprint of *Acta Astronautica* 93, 418-429 (2014) with some typographical errors corrected.

A Laser-Optical System to Re-enter or Lower Low Earth Orbit Space Debris

Claude R. Phipps
Corresponding Author, Photonic Associates, LLC, 200A Ojo de la Vaca Road, Santa Fe NM 87508, USA,
+1-505-466-3877, crphipps@photonicassociates.com

Abstract. Collisions among existing Low Earth Orbit (LEO) debris are now a main source of new debris, threatening future use of LEO space. Due to their greater number, small (1 – 10cm) debris are the main threat, while large (> 10cm) objects are the main source of new debris. Flying up and interacting with each large object is inefficient due to the energy cost of orbit plane changes, and quite expensive per object removed. Strategically, it is imperative to remove both small and large debris. Laser-Orbital-Debris-Removal (LODR), is the only solution that can address both large and small debris. In this paper, we briefly review ground-based LODR, and discuss how a polar location can dramatically increase its effectiveness for the important class of sun-synchronous orbit (SSO) objects. With 20% clear weather, a laser-optical system at either pole could lower the 8-ton ENVISAT by 40km in about 8 weeks, reducing the hazard it represents by a factor of four. We also discuss the advantages and disadvantages of a space-based LODR system. We estimate cost per object removed for these systems. International cooperation is essential for designing, building and operating any such system.

Key words: space debris, laser ablation, laser-produced plasma

1 INTRODUCTION

Space debris events are increasingly frequent. The instability predicted by Kessler and Cour-Palais [1] has now reached the point where mutual debris collisions will soon become the dominant debris-generating mechanism. While improved debris tracking and orbit prediction can temporarily improve threat avoidance via maneuvering [2,3], effective debris-clearing strategies will be necessary.

Four catalogued events have now occurred in which a debris collision terminated an active satellite. Thirty-five catalogued satellite breakups are of unknown cause, and many of these are surely due to collisions with untracked debris. However, the main urgency is to mitigate future risks. More than one hundred 1400-kg Cosmos 3M third stages with up to 300kg of residual propellant are still in LEO and MEO orbits, waiting to spontaneously explode, as they have five times. The eight-ton ENVISAT is an important threat to SSO objects. Based on [4], we estimate the cumulative probability of its debris-induced failure at 8%/decade. ENVISAT's catastrophic failure would jeopardize use of sun-sync orbits, and threaten the region below 766 km in the long term. It will take a decade to implement an effective ODR system, so now is the time to begin.

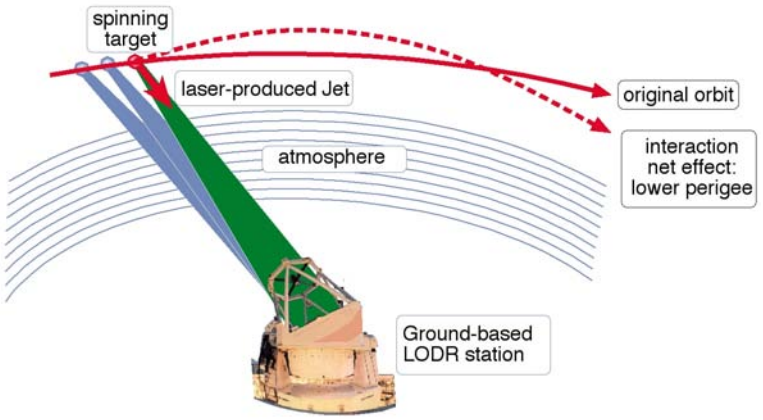

Figure 1. Classic Laser Orbital Debris Removal (LODR). A focused, 1.06-μm, 5ns repetitively-pulsed laser beam makes a jet on the object, slowing it and lowering its perigee. In cases of interest, pushing "up" on the object also lowers its perigee. The result is re-entry and burnup. A 2–3% velocity reduction is sufficient to re-enter most LEO objects.

2 LEO DEBRIS THREAT CATEGORIES

More attention has been given to re-entering the large debris, such as one-ton spent rocket bodies, than to re-entering the small ones, because that problem seems more amenable to aerospace solutions.

Large debris must be removed. They are the main source of additional debris when hit. Small debris must also be removed. They are much more numerous and so are the main threat because of the additional debris they create when they collide with a larger object. These were the main conclusions of a 45-student study at the International Space University [5]. The chance that small debris will strike a large LEO space asset is 45 times as high as the hazard from large objects [6]. Table 1 summarizes these conclusions [5, 6].

Table 1: LEO Debris Categories

LEO Debris	Small	Large
Size (cm)	1-10	10-100
Accessible Targets	100k	2.2k
Numerical Ratio	45	1
Characteristic	Main threat	Main source

3 PROPOSED SOLUTIONS

3.1 Mechanical Interaction

Solutions that have been proposed include chasing and grappling the object, attaching electrodynamic tethers, deploying nets, and deploying clouds of frozen mist, gas or blocks of aerogel in the debris path to slow the debris. Each of these is difficult to implement, costly and addresses only one or a few objects at a time. For example, an aerogel "catcher's mitt" solution designed to clear the debris in two years would require a slab 50cm thick and 13km on a side. Such a slab would weigh 80 kilotons and cost $1T to launch [6]. Another problem is the steady 12kN average thrust required to oppose orbital decay of the slab against ram pressure, even in an elliptical orbit.

Few concepts have progressed to the point where accurate costs can be calculated, but Bonnal [8] has estimated a cost of 13 - 17M$ per object for deorbiting large targets. Any mechanical solution will involve a comparable Δv from Earth, so we take this estimate as representative of removal cost per large item with mechanical methods.

3.2 Laser Interaction Categories

Laser-based methods can be divided into three general categories distinguished by their goals and laser beam parameters. At low intensities below the ablation threshold, lasers have been proposed to divert debris through light pressure [9]. In this case, the proposed hardware arrangement will deliver at most a few times the intensity of the sun to the debris, and that only during a few minutes' time while the debris passes above the laser site, rather than all day, so that sunlight produces a much larger time-integrated effect. This method does not effectively address the debris growth problem. At higher laser intensity, we can consider continuous (CW) laser ablation, but the slow heating and decay characteristic of CW thrust on tumbling debris will normally give an ablation jet whose average momentum contribution cancels itself. CW heating causes messy melt ejection rather than clean jet formation, possibly adding to the debris problem, and CW lasers cannot reach the required intensity for efficient coupling to targets at the ranges involved without a very small illumination spot size, requiring an unacceptably large mirror. This is why we have chosen pulsed lasers for the problem (Figure 1).

A NASA headquarters concept validation study [10] concluded that the idea of using pulsed lasers to remove essentially all dangerous orbital debris in the 1 – 10cm range between 400 and 1100 km altitude within two years was feasible, and that its cost would be modest compared to that of shielding, repairing, or replacing high-value spacecraft that would otherwise be lost to debris.

4 GROUNDBASED LODR OVERVIEW

4.1 Momentum Transfer Theory

Anyone who has aligned a pulsed laser beam using apiece of black photo paper has heard and felt the "pop" due to laser momentum transfer. This is one of the few examples of action without reaction on the source.

The figure of merit for pulsed laser ablation is the mechanical coupling coefficient C_m, which relates the impulse delivered to the target by the laser ablation jet to the laser pulse energy required to produce the jet on its surface:

$$C_m = p\tau/\Phi = p/I \text{ N/W}. \quad (1)$$

In Eq. (1), p is the ablation pressure delivered to the target by a laser pulse with intensity I and duration τ, and laser fluence Φ (J/m^2) = $I\tau$. C_m values for laser ablation are well-known for many materials [11, 12], and are about four orders of magnitude larger than the effect of light momentum (C_{mhv} = 2/c = 6.7 nN/W). Hot vapor or plasma is created by the interaction, not new debris.

As incident pulsed laser intensity I increases in vacuum, vapor is formed and C_m rises rapidly to a peak, then gradually decreases according to

$$C_m = C_{mo}/(I\lambda\sqrt{\tau})^{1/4} \quad (2)$$

above the vapor-to-plasma transition, because more energy is going into reradiation, ionization, and bond breaking than to propulsion.

The parameter C_{mo} is primarily a function of the average atomic mass A and charge state Z in the laser produced plasma above the surface [12], rather than of the surface optical reflectivity at the laser wavelength. This is because the plasma mediates energy transfer from the laser to the surface. For a 1.06μm, ns-pulse laser incident on a target, the center wavelength reaching the surface can well be in the hard ultraviolet.

For a singly ionized plasma [Z=1], C_{mo} varies from 75 – 200N/MW as the target material changes from hydrocarbon with $A \approx 6$ to iron or, from 45 – 120N/W for Z=3. An approximate relationship for the optimum fluence Φ_{opt} where this peak occurs, for a range of metallic and nonmetallic materials, is given Eq. (3) with a robust value B = 8.5E8 J/m^2 for robust coupling (about twice the value in refs. [11 – 13]).

$$\Phi_{opt} = B\sqrt{\tau} \text{ J/m}^2 \quad (3)$$

for τ>100ps. For example, with an 8ns pulse, $\Phi_{opt} \cong 75$ kJ/m^2. Alternatively, we can combine (2) and (3) to find

$$(I\lambda\sqrt{\tau})_{opt} = 8.5E8\lambda\,. \quad (4)$$

This gives $(I\lambda\sqrt{\tau})_{opt}$ = 900 W m^{-1}s$^{1/2}$ for the location of the peak coupling when λ = 1.06μm and τ=8ns, in good agreement with Figure 2 of [6]. We note that a strong advantage exists for going to the UV, if C_{mo} is fixed.

Finally, substituting Eq. (4) into Eq. (2) gives an estimate of the optimum coupling value C_{mopt} one might expect for various materials, plasma ionization states and laser parameters (Table 2). We find similar measured values in the literature [12, 14-17] at or near 1.06μm and 8ns, the case for this study. For multi-layer insulation (MLI, aluminum-coated kapton), we might expect $C_{mopt} \approx 60$ N/MW.

Table 2. Typical Impulse Coupling Coefficients (8ns, 1.06μm)

Material	C_{mopt} (N/MW)	Ref
Polyethylene, Kapton®	50	12
Aluminum Alloys	75	14 - 16
Kevlar®	160	17

In order to calculate deliverable $(I\lambda\sqrt{\tau})_{opt}$ on a target at range z, we first need to consider beam spread due to diffraction. The beam spot diameter d_s at the target is

$$d_s = aM^2\lambda z/D_{eff}\,, \quad (5)$$

where M^2 is the beam quality factor (1 is perfect) and D_{eff} is the effective illuminated beam diameter at the LODR output aperture D for calculating diffraction. For example, with a hypergaussian with index 6 generated by a LODR system with corrected beam quality M^2 = 2.0 (Strehl ratio S = 1/M^2 = 0.25), D_{eff}/D = 0.9 and a = 1.7.

The product WD_{eff}^2 required to deliver fluence Φ to the target is given by [6]

$$WD_{eff}^2 = \frac{\pi M^4 a^2 \lambda^2 z^2 \Phi}{4T_{eff}}. \quad (6)$$

In Eq. (6), W is laser pulse energy (J) on the target and the effective transmission from the LODR aperture to the target T_{eff} is the product of all system losses, including apodization, obscuration and atmospheric transmission.

W is bounded above by the fluence that excites nonlinear optical losses in the atmosphere while the beam is still close to the source. This limit is primarily set by stimulated Raman scattering [6, 18]:

$$W/D^2_{\text{eff}} = 2.36\text{E}16\ \lambda\tau \quad (7)$$

for pulses longer than 100 ps. Combining all these relationships gives the interesting result that

$$W = 4.0\text{E}12\ aM^2 \lambda^2 z\ \tau^{3/4}/T^{1/2}_{\text{eff}}, \quad (8)$$

which shows that the required pulse energy W increases less than linearly with pulse duration and linearly, (as against the usual expectation that it varies quadratically), with range. For the large target work reported in this paper, we will select a value of d_s that is larger than the diffraction limited result in order to make system design less critical.

For continuity, we defer discussion of target acquisition and tracking to section 5, discussing the debris removal strategy first.

Inverting Eq. (6), the delivered fluence given the other parameters is

$$\Phi = \frac{4WD_{eff}^2 T_{eff}}{\pi M^4 a^2 \lambda^2 z^2}. \quad (9)$$

4.2 Orbit Modification

With λ = 1.06 μm, z = 1000 km, T_{eff} = 0.5 and M^2 = 2.0, τ = 8 ns and a = 1.7. Eq. (8) gives W = 18 kJ and Eq. (7), D_{eff} = 9.4 m. These are typical numbers for the ground-based LODR system.

We use an efficiency factor η_c for the combined effects of improper thrust direction on the target, target shape effects, tumbling, etc. in reducing the laser pulse efficiency in producing the desired velocity change,

$$\Delta v_{||} = \eta_c C_m \Phi/\mu. \quad (10)$$

More precise laser-ablation induced orbit change calculations are given in [6], In Eq. (10), μ is the target areal mass density (kg/m^2). This formulation makes it easy to account for laser beam "overspill" for small debris, without having to specify the actual size and mass of each target. We take η_c = 0.3 after Liedahl et. al. [19]. A detailed treatment of debris shape factors and their effect on coupling appears in [19] and [20].

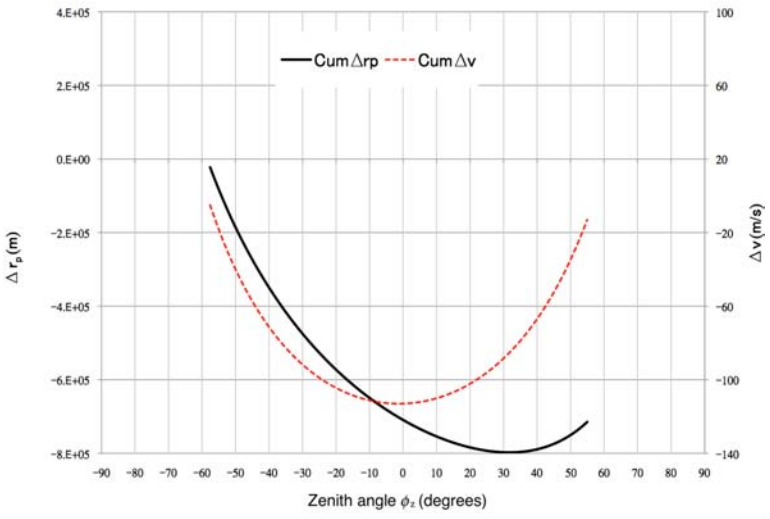

Figure 2. Perigee reduction and velocity change vs. zenith angle ϕ_z for small targets. (Color online)

4.3 Small LEO Target Re-entry [Groundbased, Equatorial Station]

In a typical case, $|\Delta v_o|$ = 150 m/s for re-entry. Modeling has shown the surprising result that pushing "up" on the debris (when it is near apogee) can also lower its perigee, as well as can pushing "back" against the direction of travel. This means that the useful range of target zenith angles (from Earth surface) for applying the laser beam can extend past the vertical to +30°. In Figure 2, target re-entry is achieved in one pass for any target smaller than the 31-cm diameter laser spot at 1000 km range, with areal mass density 10 kg/m^2 or less [6]. Single

pass re-entry of small targets is critical in the small debris problem for eliminating post-shot tracking.

The largest target re-entered under the Figure 2 conditions has 0.75 kg mass. For this case, wavelength is 1.06μm, pulse energy 10.9kJ, and pulse repetition rate 14Hz. In this case, initial orbit perigee is –120 degrees geocentric (upstream, from Earth center) relative to the laser site, and 2010 pulses are applied over 144s to achieve 200km perigee, which we consider equivalent to re-entry. Details of the momentum coupling calculation are provided in [6]. A more optimal small target case is outlined in Table 3.

Table 3. Small Target Re-entry, Groundbased Equatorial Station

Target Parameters		**Optical System Parameters**	
Mass [nonspecific target] (kg)	0.75	Wavelength λ (μm)	1.06
Perigee (km)	1,000	Pulse Length τ (ns)	5.0
Apogee (km)	1,015	Spot Size on Target (cm)	31
Repeat Period [nonspecific orbit] (days)	10	Pulse Energy (kJ)	8.5
Operating Fraction [clear weather etc.] (%)	80	Momentum Coupling Coefficient (μN-s/J)	75
Number of Passes for Re-entry	1	Pulse Repetition Frequency (Hz)	13
Time to Re-enter one Target (s)	200	Push Efficiency η_c	0.30
Primary Mirror Diameter (m)	13	Fluence on Target (kJ/m^2)	75
Average Interaction Duration (s)	200	Beam Quality Factor	2.0
Cost per Object Removed (k$)	**12**	Number of Objects Removed per year	20,000
k$/kg Removed	**16**		

The costs listed in this paper are estimates only, based on the LODR system cost model in [10] for a complete system which we amortize in four years. They may be in error by a factor of two, but are useful for comparing systems. In Table 3, we assume we can re-enter 100 different targets per day, with 200 days per year operation.

4.4 Large Target Re-entry [Groundbased , Equatorial Station]

Table 4. Generic Large Target Re-entry, Groundbased Equatorial Station

Target Parameters		**Optical System Parameters**	
Target Mass (kg)	750	Wavelength λ (μm)	1.06
Perigee (km)	800	Pulse Length τ (ns)	8.0
Apogee (km)	800	Spot Size on Target [deliberately defocused] (cm)	65
Repeat Period (days)	10	Minimum Spot Size (cm)	29
Operating Fraction [clear weather, etc.] (%)	80	Pulse Energy (kJ)	39
Number of Illuminated Passes for Re-entry	108	Momentum Coupling Coefficient (μN-s/J)	75
Time to Re-enter Target (yrs)	3.7	Pulse Repetition Frequency (Hz)	8.8
Primary Mirror Diameter (m)	15	Push Efficiency η_c	0.30
Average Interaction Duration (s)	250	Fluence on Target (kJ/m^2)	75
Cost per Object Removed (M$)	**4.7**	Beam Quality Factor	2.0
k$/kg Removed	**6.3**	Number of Objects Removed	750

It has been claimed that lasers cannot de-orbit large, one-ton debris objects. Indeed, single-pass re-entry of large objects is not practical. However, given many overhead passes, Table 4 shows the expected performance of a 9 Hz, 39 kJ, 1.06 μm laser re-entering a generic 750 kg target, using an equatorial laser station with a 15m diameter aperture. Calculations are described in detail in [6].

A 4-minute interaction period combines with opportunities averaging once per ten days to give 44 months for re-entering this generic target. As we will show later, lasers can more quickly raise or lower orbits to lower-risk regions without re-entry. For these generic large targets, we assume a repeat period of 10 days over our laser site. With a 250s interaction interval, plus a minute for reacquisition and pointing, a 6.4-hour operating day (8 hours with 80% operating fraction) offers the possibility to address at least 75 unique targets in parallel each day, so that a total of 750 such large

objects may be re-entered in the four years it takes to re-enter one, at an estimated cost of $4.7M each. These results require patience, and although the cost per object removed is estimated to be 3-4 times less than that for the standard mechanical solutions mentioned in section 3.1, these costs may turn out to be more nearly equal due to the uncertainties involved in both. However, this system can be addressing large and small targets simultaneously, which the standard approach cannot. Recall that it is only necessary to re-enter 15 of these large objects annually to *stabilize* the debris environment [21]. From this standpoint alone, a pulsed LODR system is expected to be a good investment.

4.5 Groundbased Target Access Rate

Table 5. Groundbased detection rate vs. whole array FOV (800km range, 300 SSO targets)

d_{fov} (km)	Half angle θ (deg.)	Solid angle Ω (sterrad)	Access rate, targets /hr
25	0.9	0.0008	0.49
30	1.1	0.0011	0.59
50	1.8	0.0031	0.98
70	2.5	0.0060	1.4
100	3.6	0.012	2.0
150	5.4	0.028	3.0

Access is the first step. If the target is not in the field of view, we cannot acquire it. For the groundbased acquisition system, the target access rate $\dot{N}$ is linearly proportional to the debris areal density (number per unit area) and to the diameter d_{fov} of the field of view (FOV). Debris may be entering the FOV from any direction.

The number of debris within the FOV is proportional to its area, but the rate at which they enter the FOV solid angle Ω is proportional to the FOV perimeter and the velocity with which they cross the perimeter, not the area of the FOV. This is counter-intuitive, but can be understood either dimensionally:

$$\text{Number/s} = \text{number/km}^2\text{*km/s*km} \tag{11}$$

or by imagining unfolding the FOV perimeter into a straight line segment and counting the rate at which a one-dimensional debris cloud crosses the line. Slewing the acquisition FOV can increase the detection rate, but adds unneeded complexity to this discussion. For this case, it can easily be shown that, for N uniformly distributed targets at altitude h (km) with Earth radius R_E (km), orbital velocity

$$v_o = \frac{632}{\sqrt{R_E + h}} \text{ km/s.} \tag{12}$$

For an array with FOV slewing at speed v_s at range, looking at objects moving with velocity v_o, we can show

$$\left[\frac{\dot{N}}{N}\right]_g = \frac{(v_o + v_s)d_{fov}}{4\pi(R_E + h)^2} E\left[\frac{2\sqrt{v_o v_s}}{(v_o v_s)}\right] = \frac{v_o d_{fov}}{8(R_E + h)^2} \qquad \text{for a staring array } [v_s = 0]. \tag{13}$$

In Eq. (13), E is the complete elliptic integral of the second kind. At altitude h = 800km, v_o=7.5 km/s, and $\dot{N}/N$ = 1.8E-8 d_{fov} s^{-1}. If we want to access a class of 300 SSO objects in this altitude band and d_{fov}=100km, we will see them at least every 30 minutes for a 0.012 sterrad FOV solid angle [Table 5] if they were uniformly distributed around the equator. Access rate would be 330 times larger for the 100k accessible small targets. For the d_{fov}=100km case in Table 5 and a state-of-the-art 100Mpixel array, d_{sp}=10 m for one pixel.

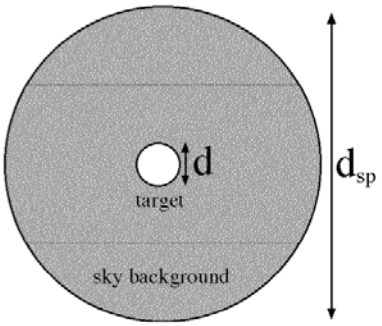

Figure 3. Diameter d_{sp} is defined as the footprint of one pixel at range z

4.6 Passive Acquisition and Tracking

Acccess is not acquisition. Acquisition implies not only target access, but achievement of adequate signal to background ratio S/B and adequate photoelectron number N_{pemin} per detector array pixel. We take N_{pemin}=10.

Useful tracking implies only predicting the position of a debris object to within a d_{sp} = 10m uncertainty for handoff to the active tracking system associated with the "pusher laser," [section 4.7].

In [6], we describe a system that can achieve this. Here, we review the requirements for acquisition and tracking in more detail.

We will assume multiple, broad FOV staring acquisition telescopes with tens of cm aperture and a large, curved focal plane array with high quantum efficiency and high pixel density using solar target illumination of the target. This part of the system is limited to about 2-3 hours operation per day at dawn or dusk when the target is illuminated by the sun in a mostly dark sky, so we need a network of such telescopes distributed around the Earth to establish accurate track predictions which can be sent to the single pusher laser location. No adaptive optics are assumed for acquisition.

We can choose the field of view of a single acquisition array pixel to give an adequate signal to background ratio *S/B*, where *R* is the target's diffuse reflectivity into π sterrad. Figure 3 explains diameters *d* and d_{sp}, the latter of which is defined as the FOV of one detection array pixel.

$$S/B = RI_\lambda/B_\lambda(d/d_{sp})^2 \tag{14}$$

Typical values for background and source irradiance B_λ and I_λ are given in Table 6 [22-24]. I_λ is source brightness due to solar radiation.

Table 6. Source and Background Brightness on the Earth within 15 degrees of zenith, full moon

Site/Time of Day, Line of Sight	Center Spectrum λ	Spectral Brightness $B\lambda$ ($Wm^{-2}sr^{-1}\mu m^{-1}$)	Source Brightness I_λ ($Wm^{-2}sr^{-1}\mu m^{-1}$)
Typical/Clear Twilight, Vertical	550nm	5.0E-4	1000
Typical/Clear Night, No Moon, Vertical	550nm	5.0E-6	
Typical/Clear Night, Moon, Vertical	550nm	5.0E-5	

Putting these numbers together for several aperture sizes D_b, we get results shown in Table 7, where we only consider cases for which *S/B* >10 and N_{pe}>10. The second condition for successful acquisition is achieving an adequate number of photoelectrons N_{pe} per telescope array pixel, after achieving adequate S/B,

$$N_{pe} = \frac{d_{sp}T\eta_c\pi I_\lambda\Delta\lambda}{16v_o z^2(hc/\lambda)}(dD_b\sqrt{R})^2 \tag{15}$$

In Eq. (15), the new parameters are photon energy hc/λ, target velocity v_o transverse to the field of view, atmospheric transmission *T*, detector photoelectric efficiency η_e, and optical bandwidth $\Delta\lambda$. For the groundbased system, on Earth, we choose a 13μrad field of view for any visible wavelength aperture larger than 10 cm because these telescopes will not have adaptive optics (AO), and this is the size of a VIS-λ turbulence cell without AO. Because turbulence is random, it is also possible, at a lower data rate, to have much better "lucky seeing" in a snapshot. However, this will not eliminate first order "tilt" in the wavefront, and may not be useful for establishing tracks for the pusher laser.

Table 7. Groundbased *S/B* and N_{pe} at 550nm with Various Target and Mirror Sizes
[z=800km, $v_{o\perp}$=7.5km/s, pixel FOV=13μrad assumed due to uncorrected atmospheric turbulence, d_{sp} = 10m is target position uncertainty. "Night" and "twilight" are on the ground]

Debris *d* (cm)	FOV, μrad	$D_b d\sqrt{R}$	N_{pe} per 13μm pixel	Aperture D_b(m)	Reflectance *R* (π sr)	*S/B* (night)	*S/B* (twilight)
100	13	1	7.2E5	0.50	0.25	8.0E6	8.0E4
100	13	0.5	1.8E5	1.0	0.25	5.0E5	5000
10	13	0.025	450	0.5	0.25	5000	50
10	13	0.05	1800	1.0	0.25	5000	50
1	13	0.019	260	2.0	0.90	180	1.8

"Background" illumination comes mainly from a spot whose average distance from the ground is 3.5km, not 800km, with diameter proportional to the FOV diameter at that altitude, much less than d_{sp}. Above the atmosphere, zodiacal and diffuse galactic light contribute only 3.4E-7 $Wm^{-2}sr^{-1}\mu m^{-1}$ in the visible, ten times less than the smallest B_λ in Table 6. We did not take account of that. Near cities, conditions will be much worse. Modest size mirrors handle most debris.

4.7 Handoff to Active Target Acquisition for a Groundbased System

Table 8. Signal to Background Ratio in Groundbased Daylight Active Acquisition

Target dia. (m)	Laser photons on target	Signal photons received (S)	Background photons received after 0.19nm filter and 75km range gate (B)	S/B
0.015	1.05E15	1.85E4	1.5E4	1.2
0.02	1.87E15	3.28E4	1.5E4	2.1
0.05	1.17E16	2.05E5	1.5E4	13
0.1	4.67E16	8.21E5	1.5E4	53
0.2	1.87E17	3.28E6	1.5E4	210
0.5	1.17E18	2.05E7	1.5E4	1320
1.0	4.67E18	8.21E7	1.5E4	5300

In the generic groundbased acquisition system, with a field of view 100km in diameter at 800km range, considering all targets, 2 -3 objects per minute will pass through the field of view, more than enough input. Multiple acquisition systems around the Earth ensure that several of them will see the target in daylight while they are in darkness, and be able to establish a track that can be projected to the pusher laser location with 10–20m uncertainty.

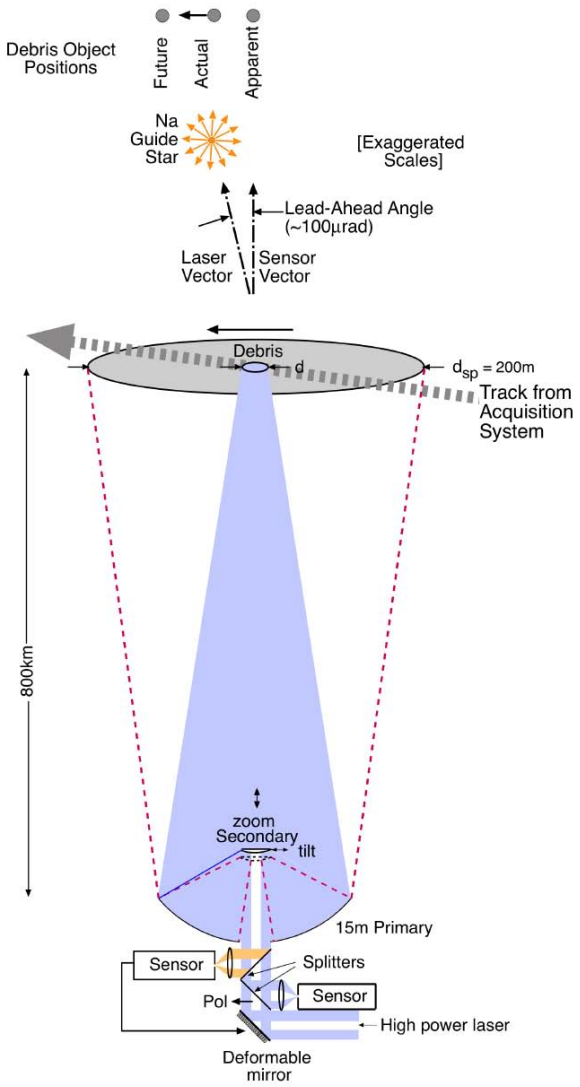

Figure 4. Illustrating Handoff to Active Tracking, Groundbased System.

It is then necessary to reduce this uncertainty to the order of 10cm. We do that with active acquisition, using the "pusher laser" system and its adaptive optics, and taking advantage of its 15m diameter mirror as a receiver. After a target track has been passed to it, the high power LODR system (initially defocused) illuminates a d_{sp}=200m region containing the track established by the acquisition network (Figure 4). This is critical, so that the LODR system has time to accelerate to the target angular velocity and location. With the large (15m) receiving aperture, 35kJ pulses from the pusher laser will generate enough scattered photons to see small targets (Table 8). The system then progressively focuses until the target return shifts into the blue, indicating that a plasma has been formed. Active acquisition is possible even in daylight with range binning and spectral filtering [6, 10]. The accuracy of the U.S. Space Surveillance System would also be considered in determining a value of d_{sp} for this activity. In Figure 4, the splitters are polarization selective. The outgoing beam is not attenuated, but 50% of the randomly polarized target return goes to the sensors.

For daylight active acquisition (Table 8), we assume λ =1.06μm, target range z = 800km, laser and detector filter bandwidth $\Delta\lambda$ = 0.19nm, corresponding to the 50GHz NIF bandwidth, handover from acquisition system d_{sp} = 200m, daylight B_λ = 25 $Wm^{-2}sr^{-1}\mu m^{-1}$ at 60° from zenith [25], laser pulse energy W = 35kJ, LODR system mirror diameter D_{eff} =15m, range gate Δz =75km (250us), target albedo (diffuse reflectance) R =0.5 into π steradians and array quantum efficiency η_{pe}=80%.

InGaAs focal plane arrays now have quantum efficiencies of 80% [26]. In our active tracking system, a 5-cm Lambertian scattering target with diffuse reflectivity R =

0.5 into π steradians at 800 km range would return about 2E5 photons to its array pixel on the ground, with a signal to day sky background ratio of 78, on the particular detector pixel to which laser photons returned. The system would require a bandwidth of 0.2nm for both the laser and narrowband optical filter, and a 75 km "range gate." Using a 100 Mpixel array with a 200m field of view, each pixel projects onto a 2cm spot at range in space. Multiple independent adaptive optics systems are required for the laser itself and atmospheric turbulence correction.

The narrowband optical filter is easy to obtain. Range gating amounts to reading out the array every 250μs and storing the data in slices, delayed from laser firing by the propagation time. This activity by itself gives rough range information.

In Figure 4, "look-ahead" refers to the fact that a computational algorithm must be used to point the pusher laser to where the target will be a time *z/c* after it is detected, corresponding to a displacement of about 20m.

5. NEW IDEAS

5.1 Polar Station for Very Large SSO Target Re-entry or Orbit Lowering

A polar location, for example, at the Amundsen Station, 0° from the South Pole, or at the Alert Station, Nunavut, Canada, 817 km (8°) from the North Pole will dramatically increase the interaction frequency for SSO large debris objects. Table 9 shows that a majority of these types of orbits lie within 8° of the pole [27-28], and have a useful zenith angle of 40 – 50°. At the poles [Figure 5, Table 9], we have a "shooting gallery" in which SSO targets of interest pass overhead 14 times a day rather than once every 10 to 35 days. If we assume a 20% operating duty cycle due to weather effects, we still have a factor of 50 better target access rate for these targets than for the equatorial station.

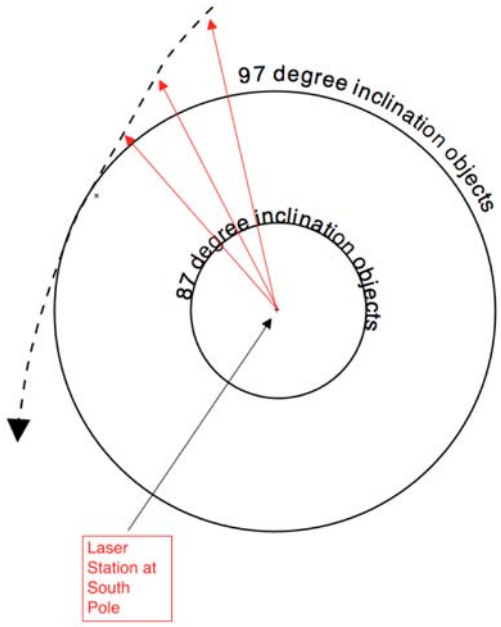

Figure 5. View Looking Up at the South Pole

Table 10 shows a quantitatively different result from those given in Table 4. With a polar LODR station, we can re-enter a defunct Cosmos3M in 60 days. A 250s interaction interval, plus a minute for reacquisition and pointing, a 1.6-hour operating day (8 hours with 20% operating fraction) and a 100-minute repeat period together offer the possibility to address at least 19 unique targets in parallel during each day, re-entering them all in two months. Three hundred such targets would then require 300/19 x 2 = 32 months to re-enter, at a cost per unit of 5.3M$, based on three years' total operation of the laser station on this type of target.

Finally, Table 11 shows that we also need only two months rather than 3.7 years to lower ENVISAT 40 km. If we devoted the LODR station to this purpose, 60 days of operation would cost 200M$. However, this use would represent

Table 9. Zenith Angles at the Poles for Representative SSO Debris Objects

Major Inclination Clusters (+/- 2°)	Radians from Pole	Representative Debris	Min Alt (km)	Max Alt (km)	Distance from Polar Axis (km)	Zenith Angle from Pole (deg)
83	0.12	Meteor, Gonets	600	1000	850 - 899	42-55
90	0.00	Thor Ablestar, Scout	700	1300	0	0
97	0.12	Cosmos, Delta	600	900	850 - 887	45-55
99	0.15	ENVISAT	767	767	1056	54

only a 6% duty cycle, so we consider the cost of lowering ENVISAT to be 11.5M$, because the station can be used for

Table 10. Large SSO Target Re-entry, Groundbased Polar Station [Cosmos 3 example]			
Target Parameters		**Optical System Parameters**	
Target Mass (kg)	1,400	Wavelength λ (μm)	1.06
Perigee (km)	800	Pulse Length τ (ns)	8.0
Apogee (km)	800	Target Spot Size [deliberately defocused] (cm)	65
Repeat Period (days)	0.07	Minimum Spot Size (cm)	29
Operating Fraction [clear weather, etc.] (%)	20	Pulse Energy (kJ)	39
Number of Illuminated Passes for Re-entry	192	Momentum Coupling Coefficient (μN-s/J)	75
Time to Re-enter Target (days)	66	Pulse Repetition Frequency (Hz)	9.3
Primary Mirror Diameter (m)	15	Push Efficiency η_c	0.30
Average Interaction Duration (s)	250	Fluence on Target (kJ/m^2)	75
Cost per Object Removed (M$)	**5.3**	Beam Quality Factor	2.0
k$/kg Removed	**3.8**	Number of Objects Removed	300

other things during clear weather.

Table 11. Large SSO Target 40km Lowering, Polar Station [ENVISAT example]			
Target Parameters		**Optical System Parameters**	
Target Mass (kg)	8,000	Wavelength λ (μm)	1.06
Perigee (km)	770	Pulse Length τ (ns)	8.0
Apogee (km)	770	Target Spot Size [deliberately defocused] (cm)	65
Repeat Period (days)	0.07	Minimum Spot Size (cm)	29
Operating Fraction [clear weather, etc.] (%)	20	Pulse Energy (kJ)	39
Number of Illuminated Passes for Lowering	192	Momentum Coupling Coefficient (μN-s/J)	75
Time to Lower Target 40km (days)	66	Pulse Repetition Frequency (Hz)	14
Primary Mirror Diameter (m)	15	Push Efficiency η_c	0.30
Average Interaction Duration (s)	250	Fluence on Target (kJ/m^2)	75
Cost to Lower ENVISAT (M$)	**7.2**	Beam Quality Factor	2.0

5.2 Spacebased LODR System

In 1991, Schall proposed a space based pulsed laser debris removal system based on the same principles as groundbased LODR [29]. There are some advantages. The concept is that, since the station is physically sweeping out space at 7.5 km/s, the laser range required to attain the same target interaction rate as groundbased LODR would be smaller, perhaps 50 - 100km, leading to smaller optics, less mass and therefore comparable or lower cost. Mass is important, because of the current 20 k$/kg cost of placing mass in LEO [6]. Over time, a station in an eccentric equatorial orbit could access all LEO orbits. Also, the interaction geometry is more favorable. In contrast with groundbased LODR, the cost and feasibility of this approach has never been studied in any detail. In this section, we compare expected performance of the two types of system.

Figure 6 illustrates space and groundbased systems. We show debris clouds moving in both directions because, for example, France launches SSO objects to the North while the U.S. launches southward.

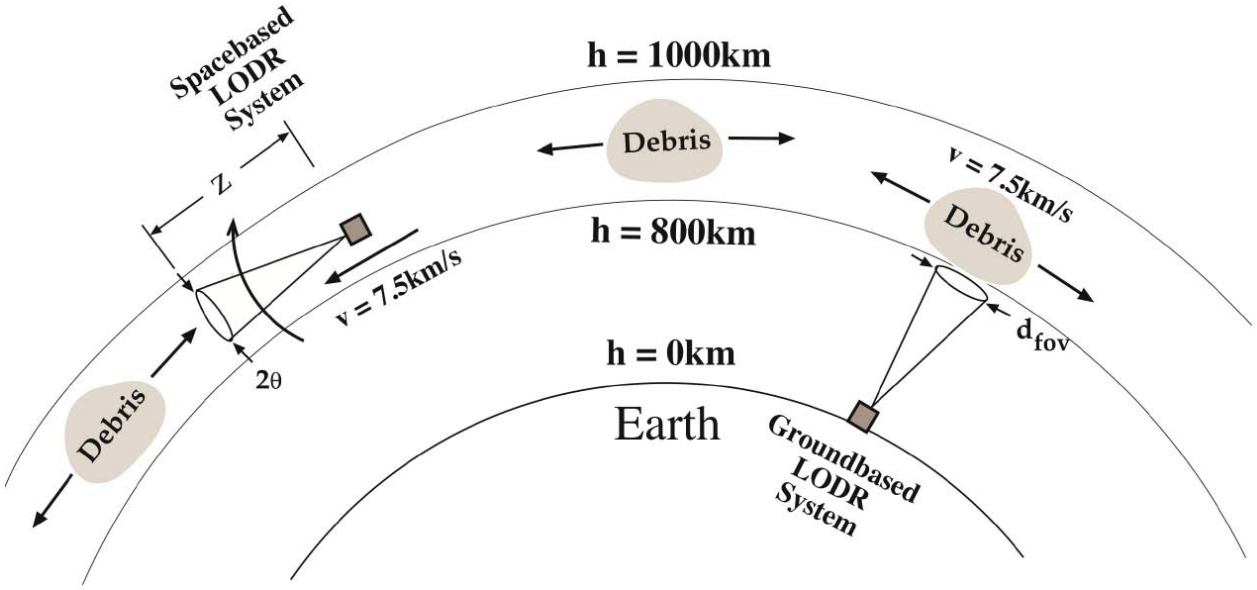

Figure 6. Comparing Space- and Ground-based LODR Systems

5.2.1 Spacebased System Target Access Rate

For the spacebased system, because of its orientation, access rate is proportional to the FOV solid angle at operating altitude, and is critically dependent on the debris and station velocity vectors (Figure 7).

If the station and debris are moving in opposite directions, we have a relatively short interval $t_{dec} = z/2v_o$ s to work on the target. For example, if z = 150km, we have t_{dec} =10s, rather than 250s as in the groundbased alternative.

Here, the important velocity is the relative one, v_{rel} and the relevant density is volumetric rather than areal. With earth radius R_E (km), orbit altitude h (km), and altitude band thickness Δh (km) and $\left|\overrightarrow{v_d}\right| \cong v_o$, we have:

$$v_{rel} / v_o = 2\sin(\theta/2) \tag{16}$$

and

$$\dot{N} / N\big|_s = v_o d_s^2 / [16(R_E+h)^2 \Delta h] \tag{17}$$

To have a good effect on target, we have a solid angle $\pi\theta^2/4$ within which the station can work effectively. To first order, including a correction for decelerating the target by an amount Δv,

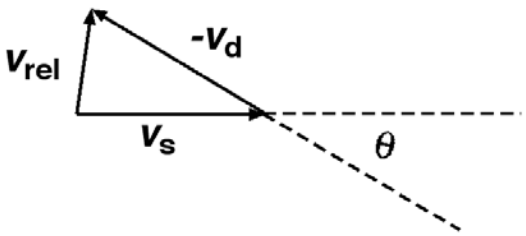

$$\theta = 2 \sin^{-1} [(2z/ t_{dec} - \Delta v)/(4v_o)] \tag{18}$$

If, for example, v_o = 7.5km/s, applied deceleration Δv = 0.15km/s, Δh = 700km, Table 12 shows the range of angles over which we could operate a spacebased system over 100s before the target is out of range, together with the operating solid angle Ω.

Figure 7. Debris, station and relative velocity vectors

Table 12. Spacebased large-target access rate (100s viewing, 300 SSO targets, desired Δv =150m/s)

Range z (km)	Half angle θ (deg.)	v_{rel} (km/s)	Solid angle Ω (sterrad)	Access rate, targets /yr
30	1.7	0.23	0.0028	0.40
50	3.3	0.43	0.010	3.9
70	4.8	0.63	0.022	17
100	7.1	0.93	0.048	75
150	11	1.43	0.11	400
200	15	1.93	0.21	1300

It is, of course, possible that we would never see such small v_{rel} values considering orbit peculiarities. We conclude that, with a 150km range, 22 degree FOV spacebased system, we can access the required number of debris in this band.

Finally, debris clearance rate depends primarily on raw power delivered to the target. For large targets, this would seem to be a disadvantage for spacebased lasers, where we hope to have a less massive system than the groundbased one. However, we can use "heat capacity" mode in the laser to get around this. For small targets, it is an advantage because less range leads to smaller spots and less beam overspill. This is even more true for the UV systems we will recommend.

For the 100,000 accessible 1-10cm small targets, the spacebased alternative has an unequaled access rate [Table 13] with 150km range. The alternative is post-shot tracking, which we wish to avoid.

Table 13. Spacebased small-target access rate (100s viewing, 100k targets, desired Δv =150m/s)

Range z (km)	Half angle θ (deg.)	v_{rel} (km/s)	Solid angle Ω (sterrad)	Access rate, targets /day
30	1.7	0.23	0.0028	130
50	3.3	0.43	0.010	1300
70	4.8	0.63	0.022	5600
100	7.1	0.93	0.048	2.5E4
150	11	1.43	0.11	1.3E5
200	15	1.93	0.21	4.3E5

A significant advantage is that space permits using ultraviolet wavelengths that would not propagate in air. Using the 4th harmonic of 1.06μm at 266nm is advantageous from a system point of view. Now, the delivered beam spot size can be four times smaller with the same mirror diameter and more consistent with target size for less spillover. With z = 150km and mirror size D_b = 1m, a 266nm wavelength laser will deliver d_s = 15cm.

Tables 14 and 15 [21-23] give the background and source brightness B_λ values for the spacebased acquisition case.

Table 14. Diffuse background B_λ in space

Source	B_λ (Wm^{-2} sr^{-1} μm^{-1})	
	Visible (0.55μm)	UV (0.26μm)
Zodiacal light	2.5E-6	
Diffuse galactic light	2.1E-7	
Total	2.7E-6	1.0E-7

Table 15. Source brightness I_λ

I_λ (W m^{-2}μm^{-1})	1000	110
At λ	550nm	266nm

As we can see by comparing Tables 6 and 14, the spacebased system will experience much less background brightness, especially in the UV.

5.2.2 Spacebased Acquisition and Tracking

Table 16 shows how well a spacebased system is suited for acquiring small debris. A 50cm diameter mirror in a system with 150km range can easily acquire and track 1cm debris. Even a 5cm diameter optic can see the large objects, and signal to background ratio is always excellent. This simple analysis does not consider more advanced techniques such as on-chip binning and gating. Active acqusition with the spacebased system is dramatically improved.

Table 16. Passive Acquisition: Spacebased *S/B* and N_{pe} with Various Debris and Aperture Sizes (λ=550nm)

[z = 150km, $\Delta t = d_{sp}/[v_{rel} \tan(\theta/2)]$ = 5.5ms, pixel FOV = 10μrad]

Debris d (m)	FOV, μrad	$D_b d\sqrt{R}$	N_{pe} /pixel	Aperture D_b(m)	Diffuse R (π sr)	*S/B*
4	10	1	4.4E6	0.5	0.25	7.2E7
1	10	0.5	1.1E6	1	0.25	4.5E6
0.3	10	0.075	2.5E4	0.5	0.25	4.1E5
0.3	10	0.15	9.8E4	1	0.25	4.1E5
0.05	10	0.013	680	0.5	0.25	1.1E4
0.05	10	0.025	2720	1	0.25	1.1E4
0.01	10	0.003	27	0.5	0.25	450
0.01	10	0.005	110	1	0.25	450

Table 17. Active Acquisition: Spacebased S/B with Various Debris Sizes (λ=266nm)

[z = 150km, Δt = z/c = 500μs, pixel FOV = 10μrad, d_{sp}= 1.5m, W=220J]

Debris dia. (m)	Laser photons on target	Signal photons received (S)	Background photons received after 2.0nm filter and 150km range gate (B)	S/B
0.015	2.9E16	5.7E3	8.2E-13	6.9E15
0.02	5.2E16	1.0E4	8.2E-13	1.2E16
0.05	3.2E17	6.3E4	8.2E-13	7.7E16
0.1	1.3E18	2.5E5	8.2E-13	3.1E17
0.2	5.2E18	1.0E6	8.2E-13	1.2E18
0.5	3.2E19	6.3E6	8.2E-13	7.7E18
1.0	1.3E20	2.5E7	8.2E-13	3.1E19

5.2.3 Handoff to Active Acquisition, Spacebased System

Table 17 gives our results for handoff to the 260nm wavelength spacebased system. In this case, we use W = 220J, η_c =50%, D_b=1m, and z=150km. The Table shows that the spacebased system has a tremendous advantage in active acquisition, with regard to S/B ratio, system pulse energy and size. Figure 8 illustrates the spacebased active acquisition geometry. Of course, there is no guidestar in this case.

Table 18. Small Target Re-entry, Spacebased 266nm Station [Equatorial, Generic]

Target Parameters		Optical System Parameters	
Mass [nonspecific target] (kg)	0.75	Wavelength λ (nm)	266
Range z (km)	150	Pulse Length τ (ns)	0.1
Laser output power (burst, kW)	480	Spot Size on Target d_{sp} (cm)	**15**
Operating Fraction [clear weather etc.] (%)	100	Pulse Energy (J)	150
Number of Passes for Re-entry	1	Momentum Coupling Coefficient (μN-s/J)	106
Time to Re-enter one Target (s)	10	Pulse Repetition Frequency (Hz)	2.2kHz
Primary Mirror Diameter (cm)	100	Push Efficiency η_c	0.50
Average Interaction Duration (s)	10	Fluence on Target (kJ/m^2)	8.5
Reacquisition interval (s)	50	Beam Quality Factor	2.0
Cost per Object Removed (k$)	**2.0**	Number of Objects Removed per month	44k
k$/kg Removed	**2.7**		

5.2.4 Small Target Re-entry, Spacebased System

Now, we reduce d_{sp} to 15cm from 150cm for target re-entry. Table 18 gives target re-entry numbers for a 150J system operating in 10s bursts at 2.2kHz (480kW), necessary to achieve single pass re-entry of debris at one target/minute. Note that a 10s burst at this power level is very consistent with short-term onboard energy storage and today's space technology. Cost per target removed is estimated to be 2k$.

We estimate the mass of the laser and optical system to be 2,000kg, and using 20k$/kg for launch cost [30], the incremental cost is just 1% for qualifying and launching the system into orbit.

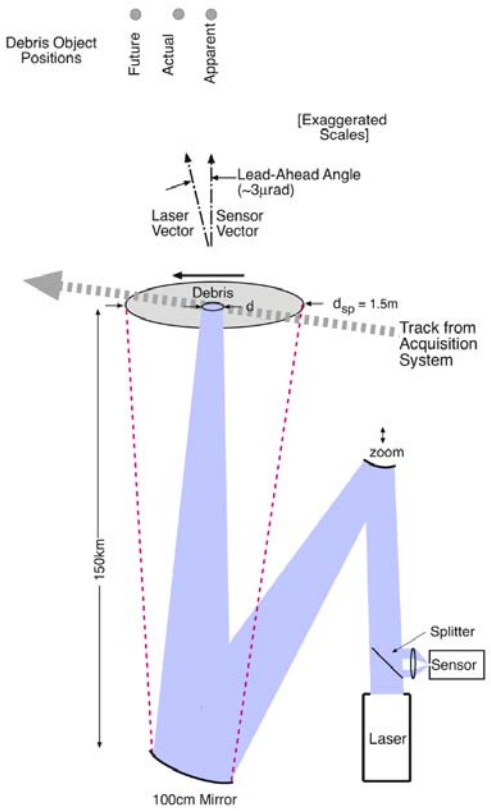

Figure 8. Active Spacebased Acquisition

6 ATMOSPHERIC TURBULENCE COMPENSATION, LASERS AND LARGE OPTICS

Phase conjugation using Stimulated Brillouin Scattering (SBS) has also been proposed for compensation atmospheric turbulence [31]. There is a lot of synergy between the system required for LODR and a laser driver for Laser Inertial Fusion Energy (LIFE) now being designed at Lawrence Livermore National Laboratory (LLNL) and with lasers being built at several European Laboratories. The high-repetition rate (10-20 Hz), high-efficiency (~12-18%) diode-pumped LIFE system will produce ~10 kJ in a single beam at 1053 nm [32]. The laser output has linear polarization, so it is easy to combine two beams into a 20 kJ per pulse laser system [33].

Techniques for making light-weight segmented mirrors have already produced the large, lightweight mirrors we require, and 39-m primaries are planned [34].

7 INTERNATIONAL COOPERATION

The most salient problem for LODR is not technical, but political. Designing, building and operating a LODR system will require international cooperation to apply the best ideas, as well as to avoid concerns that it is actually a weapon system. Also, cooperation in its operation will be needed to get permission for its use to remove specific debris objects.

8 CONCLUSIONS

We have shown that pulsed Laser Orbital Debris Removal (LODR) is more agile and less costly than mechanical debris removal techniques. It can handle tumbling objects, difficult for mechanical systems. It is the only approach that can deal with both small and large debris objects, and it will work on multi-ton objects.

The analysis reported here is unavoidably complex, because we have considered two types of targets (small, less than 1kg mass and large, up to 8,000kg) and three possibilities for LODR station location (groundbased equatorial, groundbased polar and spacebased) to address each.

In general, we conclude that the cost of removing a single piece of small debris is of order 8 – 12k$. To remove a generic large target, we expect the cost to be of order 5M$ with an equatorial station. With a polar station, we estimate 7M$ to lower ENVISAT 40km, in about two months, taking advantage of high access rate at the polar location.

A spacebased UV laser system has special advantages in rate of acquisition that drive the estimated cost for removing small debris down to 2k$. It would be done with the small debris in its +/– 100km altitude band very quickly, and so could and should be used on large debris for the remainder of its lifetime. We have not studied that option in this paper.

We estimate the incremental cost of putting a LODR system in space at about 1%, because the system is already expensive.

In building a LODR system, there are both negative and positive factors to consider (Table 19).

Each of the LODR techniques described in this paper deserves further in-depth study. Our goal in writing this paper has been to stimulate that.

Table 19. Pros and Cons for Spacebased vs. Groundbased LODR System for LEO Debris

	Groundbased		Spacebased
–	Vector geometry normally inefficient	+	Vector geometry is potentially perfect
–	Must observe sub-cm size debris during approximately 3 hours of twilight	+	Nearly fulltime observation
+	Cost of a kilogram of electro-optical equipment on the ground: about $100	–	Cost of placing a kilogram in LEO: about $20k Cost of space-qualifying a kilogram of electro-optical equipment for LEO: at least $20k.
+	Easy to repair and maintain	–	Not cost effective to repair and maintain
+	At 800km range, 0.028sterad, 1000 small targets per hour detected	–	At 150km range, 0.015sterrad, 22 small targets per day
–	Difficult to design an optical system that can see <1cm debris	+	Operating at short range, easy to see small debris
–	Restricted to 1.06μm and longer wavelengths; more diffraction, larger spot size	+	With UV wavelengths that do not propagate in air, small spots, greater momentum coupling efficiency
–	Must use adaptive optics, can never be diffraction-limited	+	Free of atmospheric aberrations, will be diffraction-limited without adaptive optics
–	Depending on site, vibrations can be a problem	+	Inertially stable platform gives high pointing accuracy
–	Background illumination much larger due to atmospheric scattering	+	Background illumination limited to galactic background
+	Electrical and laser power are both not costly on the ground	–	Debris clearance rate is dependent on total laser power, and spacebased power is expensive
–	Small but significant chance of accidental illumination of other platforms	+	Orientation and short range mean less chance of accidental illumination of other platforms

ABOUT THE AUTHOR

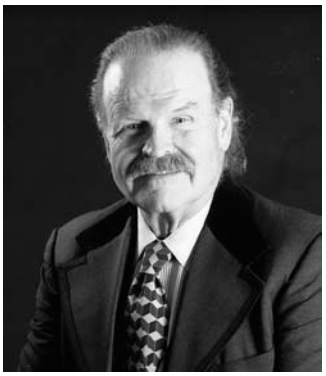

Claude Phipps earned B.S. and M.S. degrees from the Massachusetts Institute of Technology, and a Ph.D. from Stanford University in 1972. He worked in the Inertial Confinement Fusion Program at Lawrence Livermore Laboratory and, from 1974 to 1995, in the Advanced Optical Systems Group at Los Alamos National Laboratory (LANL). There, he conducted a research program on mechanical and thermal coupling of pulsed lasers to targets using high-energy-laser facilities in the United States and United Kingdom, and developed a model for vacuum laser impulse prediction. From 1994 to 1995, he was Associate Director of the Alliance for Photonic Technology at LANL. In 1995, he formed Photonic Associates, which is devoted to applications of laser space propulsion. He is the author of 110 peer-reviewed papers, 110 conference presentations including 40 invited talks, has contributed to two textbooks on laser ablation phenomena, and has organized and chaired ten symposia on high-power laser ablation.

REFERENCES

1. Kessler D. and Cour-Palais, B. (1978). Collision Frequency of Artificial Satellites: The Creation of a Debris Belt, *J. Geophys. Res.* **83**, 2637-2646
2. Henderson, J., Nikolaev, S. et al. (2010). Intelligent sensor tasking for space collision mitigation, *Proc. SPIE* **7691**, 76910L
3. Simms, L., Riot, V., et al. (2011). Optical payload for the STARE pathfinder mission, *Proc. SPIE* **8044**, 804406
4. Brudieu, P. and Lazare, B. (2012). French Policy for Space Sustainability and Perspectives, *16th ISU Symposium on Space Activities, Strasbourg*
5. Maier, P., *et al,* (2013). ISU Team Project: An Integral view on space debris mitigation and removal, *6th European Conference on Space Debris, Darmstadt 22-25 April 2013*.
6. Phipps, C. et al., (2012). Removing orbital debris with lasers, *Advances in Space Research*, **49**, 1283-1300
7. Phipps, C. (2010). Catcher's Mitt as an Alternative to Laser Space Debris Mitigation, *AIP Conf. Proc.* **1278**, 509-514
8. Bonnal, C. (2009). High Level Requirements for an Operational Space Debris Deorbiter, *Proc. NASA/DARPA International Conference on Orbital Debris Removal, Chantilly, VA*
9. Mason, J., Stupl, J., et al. (2011). Orbital Debris Collision Avoidance, *arXiv:1103.1690v1 [physics.space-ph]*
10. Campbell, J., ed. (1996). *Project ORION: Orbital Debris Removal Using Ground-Based Sensors and Lasers,* NASA Marshall Spaceflight Center Technical Memorandum 108522
11. Phipps, C. (2011). An Alternate Treatment of the Vapor-Plasma Transition, *Int. J. Aerospace Innovations* **3**, 45-50
12. Phipps, C., et al. (1988). Impulse Coupling to Targets in Vacuum by KrF, HF and CO_2 Lasers , *J. Appl. Phys.,* **64**, 1083-1096
13. Phipps, C., Birkan, M., et al. (2010). Laser Ablation Propulsion, *J. Propulsion and Power,* **26**, 609-637
14. P. Combis, P., B. Cazalis, B., J. David, J., A. Froger, A., M. Louis-Jacquet, M., B. Meyer, B., G. Nierat, G., A. Saleres, A., G. Sibille, G., G. Thiell G., and F. Wagon F., (1991). Low fluence laser-target coupling, *Laser and Particle Beams* **9**, 403 – 420
15. Fournier, K. B., (2006). Fournier, LASNEX calculations of laser-coupling coefficients for Al targets, Lawrence Livermore Laboratory report UCRL-PRES-226849
16. Saleres, A., Cazalis, B, Combis, P., David, J., Meyer, B., Nierat, G., Sibille, G., Thiell, G., and Wagon, F. (1992). Couplage Thermique et Mécanique dans L'interaction Laser-Matière a Éclairement Modéré, CEA Limeil-Valenton report 4eme Trimestre
17. Afanas'ev, Yu. V.,Basov, N. G., Krokhin, O.N,Morachevskii, N. V. and Sklizkov, G. V. (1969). Gas-dynamic processes in irradiation of Solids, *Sov. Phys.Tech. Phys.* **14** 669-676
18. Phipps, C. and Sinko, J. (2010). Applying New Laser Interaction Models to the ORION Problem, *AIP Conference Proceedings* **1278**, 492-501
19. Liedahl, D., et al. (2010). Momentum Transfer by Laser Ablation of Irregularly Shaped Space Debris, *AIP Conference Proceedings* **1278**, 772-779
20. Liedahl, D., et al. (2013). Pulsed Laser Interactions with Space Debris: Target Shape Effects, *Advances in Space Research*, to be published.
21. Klinkrad, H. (2006). *Space Debris – Models and Risk Analysis*, Praxis Publishing, Chichester, UK
22. Allen, C. W. (1973). *Astrophysical Quantities*, Athlone, London
23. Wolfe, W.L. and Zissis, G.J. (1978) *The Infrared Handbook*, Office of Naval Research
24. Reilly, J. P. (1996) in Campbell, J., *op. cit.*
25. Machuga, D. W. (1993). Daytime Performance of the LAMP Rayleigh/Raman Lidar System, MS Thesis, Pennsylvania State University
26. Hansen M. and Malchow, D. (2008). Overview of SWIR detectors, cameras and applications, *Proc. SPIE* **6939**, 693901-1 - 693901-11
27. Pisseloup, A. and Colaitis, O. (2012). Active Debris Removal of Heavy Objects, Paper 8.1, *Proc. Second European Workshop on Active Debris Removal, Paris*
28. Deluca, L., Maggi, F., et al. (2013). Active Debris Removal by Hybrid Rocket Propulsion, Paper 3.4, *Proc. Second European Workshop on Active Debris Removal, Paris*
29. Schall, W. (1991). Orbital debris removal by laser radiation, *Acta Astronautica* **24**. p. 343
30. Phipps, C. (2009). *Laser Ablation and its Applications*, Springer, New York, p. 412
31. Kulagin, O., Pasmanik G., et al. (1992). Amplification and phase conjugation of weak signals, *Sov. Phys. Uspekhi*, **35**, 506–519
32. Bayramian, A., Anklam, T., et al. (2010). Compact, efficient laser systems required for laser inertial fusion energy, *Proc. Conf. Technology of Fusion Energy*

33. Rubenchik, A., et al (2010).“Laser systems for orbital debris removal,” *AIP Conf. Proc.* **1278**, pp. 347-353
34. Strafford, D., DeSmitt, S., et al. (2006). Development of lightweight stiff stable replicated glass mirrors for the Cornell Caltech Atacama Telescope (CCAT), *Proc. SPIE*, **6273**, 62730R